J. Ocean Univ. China (Oceanic and Coastal Sea Research)
https://doi.org/10.1007/s11802-024-5599-8
ISSN 1672-5182, 2024 23 (2): 415-426
http://www.ouc.edu.cn/xbywb/
E-mail:xbywb@ouc.edu.cn

Accurate Source-Receiver Positioning Method for a High-Resolution Deep-Towed Multichannel Seismic Exploration System

LI Jing[1), 2)], LIU Kai[1), 2), *], WEI Zhengrong[3)], ZHANG Liancheng[4)], LIU Yangting[1), 2)], PEI Yanliang[1), 2)], LIU Chenguang[1), 2)], and LIU Baohua[2)]

1) *Key Laboratory of Marine Geology and Metallogeny*, *First Institute of Oceanography*, *MNR*, *Qingdao* 266061, *China*
2) *Laboratory for Marine Geology*, *Laoshan Laboratory*, *Qingdao* 266061, *China*
3) *College of Ocean Science and Engineering*, *Shandong University of Science and Technology*, *Qingdao* 266590, *China*
4) *Key Laboratory of Fluid Transmission Technology of Zhejiang Province*, *Zhejiang Sci-Tech University*, *Hangzhou* 310018, *China*

(Received November 26, 2022; revised March 10, 2023; accepted April 28, 2023)

Abstract The near-seabed multichannel seismic exploration systems have yielded remarkable successes in marine geological disaster assessment, marine gas hydrate investigation, and deep-sea mineral exploration owing to their high vertical and horizontal resolution. However, the quality of deep-towed seismic imaging hinges on accurate source-receiver positioning information. In light of existing technical problems, we propose a novel array geometry inversion method tailored for high-resolution deep-towed multichannel seismic exploration systems. This method is independent of the attitude and depth sensors along a deep-towed seismic streamer, accounting for variations in seawater velocity and seabed slope angle. Our approach decomposes the towed line array into multiline segments and characterizes its geometric shape using the line segment distance and pitch angle. Introducing optimization parameters for seawater velocity and seabed slope angle, we establish an objective function based on the model, yielding results that align with objective reality. Employing the particle swarm optimization algorithm enables synchronous acquisition of optimized inversion results for array geometry and seawater velocity. Experimental validation using theoretical models and practical data verifies that our approach effectively enhances source and receiver positioning inversion accuracy. The algorithm exhibits robust stability and reliability, addressing uncertainties in seismic traveltime picking and complex seabed topography conditions.

Key words high-resolution deep-towed multichannel seismic exploration; source-receiver positioning; array geometry inversion; seawater heterogeneity; seabed slope angle

1 Introduction

Marine high-resolution multichannel seismic exploration serves as an effective method for elucidating the structural characteristics of shallow seabed sediments and quantifying their physical properties. This approach has demonstrated remarkable efficacy in marine geological disaster assessment, marine gas hydrate investigation, and deep-sea mineral exploration (Chapman *et al*., 2002; He *et al*., 2007; Vanneste *et al*., 2014; Clare *et al*., 2017; Wei *et al*., 2018; Hutapea *et al*., 2020; Xing *et al*., 2021). With the increasing demand for resources, particularly in the exploration and development of deep-sea resources such as gas hydrates, polymetallic nodules, cobalt-rich crusts, and deep-sea rare earth elements, the importance of this endeavor has been underscored.

Traditional high-resolution multichannel seismic exploration deploys seismic sources and streamers on the sea surface, leading to attenuation of high-frequency source energy by the seawater layer and impacting the lateral resolution of seismic prospecting (Breitzke and Bialas, 2003). Consequently, since the 1980s, near-seabed multichannel seismic exploration technology involving the towing of seismic high-frequency sources and streamers near the seabed has been developed for deep-water working environments. This approach reduces the first Fresnel zone radius, mitigates high-frequency energy attenuation, and enhances both vertical and horizontal resolution, addressing limitations of conventional high-resolution multichannel seismic exploration methods (Colin *et al*., 2020a).

Recent years have witnessed the development of various near-seabed multichannel seismic exploration systems, including the Deep-Towed Acoustics/Geophysics System (DTAGS) by the United States (Gettrust *et al*., 2004), the SYstème SIsmique de Fond (SYSIF) by France (Marsset *et al*., 2010; Marsset *et al*., 2014), and the Kuiyang ST2000 by China (Pei *et al*., 2022). These systems have proven suc-

* Corresponding author. E-mail: liuk@fio.org.cn

cessful in evaluating gas hydrate systems (Talukder *et al*., 2007; Wood *et al*., 2008; Kong *et al*., 2012; Ker *et al*., 2014), characterizing free gas and gas chimneys (He *et al*., 2009; Riboulot *et al*., 2018; Colin *et al*., 2020b), identifying pockmarks (Riboulot *et al*., 2013), and assessing submarine landslide hazards (Ker *et al*., 2010, 2012; Marsset *et al*., 2010). Although both DTAGS and SYSIF use a Helmholtz resonant cavity as a deep-towed seismic source, the Kuiyang ST2000 (Fig.1), the focus of this study, innovatively adopts a plasma sparker source, offering advantages such as a higher sound source level and broader frequency band (Pei *et al*., 2022).

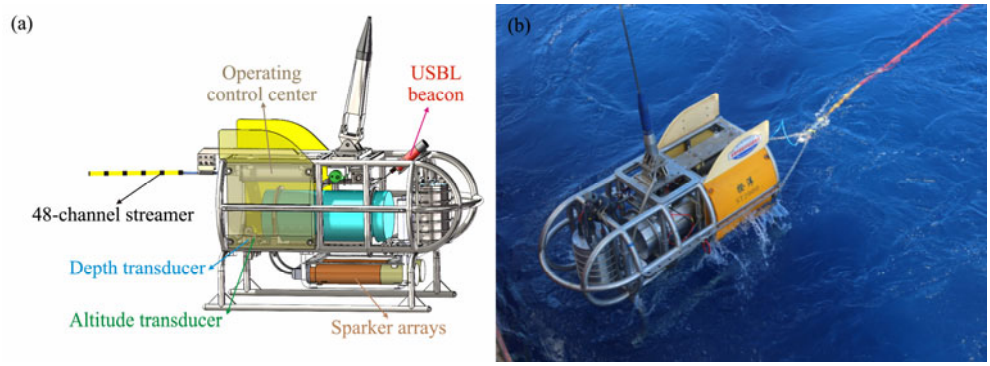

Fig.1 Deep-towed vehicle of the Kuiyang ST2000. (a), schematic; (b), actual picture.

Ensuring equipment safety and exploration quality necessitates continuous adjustment of the towing depth for a near-seabed multichannel seismic exploration system to maintain a working altitude within a certain range, typically 100–150 m above the seabed. The dynamic changes in the depth of the deep-towed seismic source and the array geometry of the streamer, influenced by ocean currents, buoyancy of the towed line array, and adjustments to towing depth, pose significant challenges in obtaining accurate source-receiver positioning information in deep water.

The acquisition of precise source-receiver positioning is a critical prerequisite for achieving in-phase stacking of effective seismic reflection waves in subsequent processing (Liu *et al*., 2022), particularly in high-resolution multichannel seismic exploration. Slight errors in source-receiver positioning can lead to hyperbolic distortion of seismic reflection waves, causing defocusing of the velocity spectrum during velocity analysis, destructive interference in the stacking process, and ultimately, seismic imaging profiles with suboptimal signal-to-noise ratios and resolutions.

In recent efforts to improve seismic imaging quality and maximize the exploration potential, scholars have proposed various source-receiver positioning methods suitable for near-seabed multichannel seismic exploration systems. For instance, in the case of DTAGS, configured with four engineering nodes along the towed line array, Rowe and Gettrust (1993) utilized linear interpolation based on depth measurements from the engineering nodes to obtain receiver positions in each shot gather. However, this method fell short of the accuracy needed for reconstructing the non-linear array geometry. Walia and Hannay (1999) calculated source and receiver depths based on the propagation path and travel time of sea-surface reflections, constraining the non-linear array geometry. On this basis, He *et al*. (2009) performed optimal inversion of engineering node positions using a genetic algorithm and derived array geometry through polynomial interpolation. For SYSIF, equipped with attitude sensors at each receiver point, Marsset *et al*. (2014, 2018) reconstructed the array geometry on the basis of the local pitch angle measurements along the seismic streamer to obtain the absolute positions of the source and receiver points. Based on the direct wave and seafloor reflection travel time, Colin *et al*. (2020a) used pitch angle measurements as initial values. They then solved the inverse problem with a local optimization method, effectively correcting the pitch angle parameters and mitigating the impact of errors in attitude sensor measurements. In summary, most existing techniques rely on attitude or depth sensor measurements of the deep-towed seismic streamer, overlooking the impact of heterogeneous seismic velocities in seawater. This oversight can lead to inaccurate source-receiver positioning, impacting the signal-to-noise ratio and resolution of deep-towed seismic imaging and potentially causing structural artifacts.

The data processing of a near-seabed multichannel seismic detection system differs from conventional high-resolution seismic data processing. In conventional high-resolution multichannel seismic exploration systems, shot points and receiver points typically remain on a relatively constant datum. However, in the case of a deep-towed multichannel seismic exploration system, the relative position relationship between the source and receivers undergoes dramatic changes. Accurate positioning information becomes paramount for exact corrections of source and receiver positions in subsequent processing, facilitating the restoration of hyperbolic characteristics in deep-towed multichannel seismic data to ensure focused velocity spectra. These steps are necessary to obtain fine and precise velocity structures, leading to the acquisition of high-quality seismic imaging profiles and information on the physical parameters of the stratigraphy.

To address these technical problems, we propose a new array geometry inversion method for deep-towed multichannel seismic exploration systems. This method is grounded in the direct wave, sea-surface reflection, and seafloor reflection travel times. It operates independently of the

attitude and depth sensors deployed along the deep-towed seismic streamer. Leveraging the particle swarm optimization algorithm, the objective function can be solved to simultaneously acquire optimized inversion results for array geometry and seawater velocity. Through experiments utilizing theoretical models and practical data, this study verifies that the proposed method can effectively improve the inversion accuracy of source and receiver positioning in deep-towed multichannel seismic exploration systems. The algorithm demonstrates robust stability and reliability, effectively addressing uncertainties in seismic travel time picking and complex seabed topography conditions.

2 Methods

2.1 Conventional Source-Receiver Positioning Method

To reconstruct the geometric shape of the array in a near-seabed multichannel seismic exploration system, we establish the relationship between the source and receiver locations and the travel time of the direct wave and sea-surface reflection, as shown in Fig.2. Utilizing seismic ray theory, the conventional source-receiver positioning method (Wei *et al*., 2020) is applied to determine the longitudinal and transverse deviations of each receiver point relative to the source, expressed by Eq. (1).

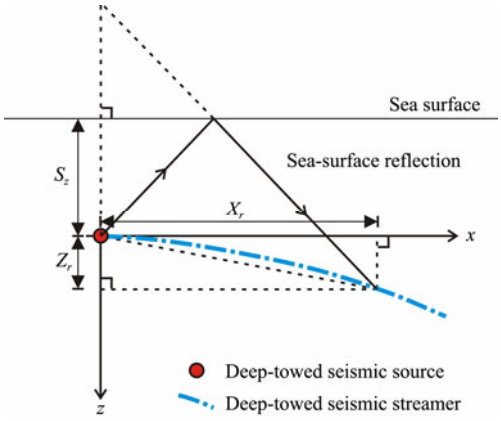

Fig.2 Schematic of the propagation path of the sea-surface reflection of the deep-towed multichannel seismic exploration system.

$$\begin{cases} Z_r = \dfrac{(t_r^{S\_\mathrm{obs2}} - t_r^{D\_\mathrm{obs2}})v_w^2 - 4S_z^2}{4S_z} \\ X_r = \sqrt{(t_r^{D\_\mathrm{obs}} v_w)^2 - Z_r^2} \end{cases}, \; r = 1,2,\cdots,N, \quad (1)$$

where S_z is the depth of the deep-towed seismic source at the current shot point, $t_r^{D\_\mathrm{obs}}$ and $t_r^{S\_\mathrm{obs}}$ are the observed values of the travel time of the direct wave and sea-surface reflection recorded at each receiver point, respectively, v_w is the seawater velocity, X_r and Z_r are the horizontal and vertical offsets of receiver point r relative to the shot point, respectively, and N is the total number of receiver points of the deep-towed seismic streamer. In previous studies, the measured value of an expandable conductivity-temperature-depth probe was commonly adopted as the reference value for seawater velocity. However, owing to the seawater heterogeneity, obtaining an appropriate seawater velocity for the entire deep-towed multichannel seismic survey line is often challenging.

2.2 Proposed Source-Receiver Positioning Method

The conventional method overlooks the constraints imposed by fixed channel spacing and the smooth curvature of the deep-towed seismic streamer. To address these limitations, in the two-dimensional case, a towed line array consisting of a deep-towed seismic source and streamer can be divided into multiple line segments using the positions of each receiver point as nodes. Based on the length and pitch angle of each line segment, the horizontal and vertical offsets of each receiver point to the shot point can be expressed as

$$\begin{cases} X_1 = l_0^x + l_1\cos\theta_1 \\ Z_1 = l_0^z + l_1\sin\theta_1 \\ X_r = X_1 + \sum_{i=2}^{r} l\cos\theta_i \\ Z_r = Z_1 + \sum_{i=2}^{r} l\sin\theta_i \end{cases}, \; r = 2,3,\cdots,N, \quad (2)$$

where l_0^x and l_0^z are the horizontal and vertical offsets of the deep-towed seismic source from the towing point of the deep-towed streamer, respectively. l_1 is the distance between the towing point and the first receiver point; l is the group interval; and θ_i and θ_1 are the pitch angles of the ith and the first line segment, respectively. X_r and X_1 are the horizontal offsets of the rth and the first receiver points from the shot point, respectively, and Z_r and Z_1 are the vertical offsets of the rth and the first receiver points from the shot point, respectively. N is the total number of receiver points of the deep-towed seismic streamer.

In addition to the direct wave and sea-surface reflection, this study introduces the traveltime of the seafloor reflection to jointly constrain the array geometry inversion of a deep-towed multichannel seismic exploration system, considering the influence of relatively complex submarine topography. Based on the schematic diagram of the propagation path of the seafloor reflection under the condition of a sloped seabed (Fig.3), the expression of the travel time of the direct wave, sea-surface reflection, and seafloor reflection acquired by each receiver point within a shot gather is:

$$\begin{cases} t_r^{D\_\mathrm{cal}} = \dfrac{\sqrt{X_r^2 + Z_r^2}}{v_w} \\ t_r^{S\_\mathrm{cal}} = \dfrac{\sqrt{(2S_z + Z_r)^2 + X_r^2}}{v_w} \\ t_r^{F\_\mathrm{cal}} = \dfrac{\sqrt{(2H_{st}^* - Z_r^*)^2 + X_r^{*2}}}{v_w} \\ H_{st}^* = H_{st}\cos\alpha \\ X_r^* = X_r\cos\alpha - Z_r\sin\alpha \\ Z_r^* = X_r\sin\alpha + Z_r\cos\alpha \end{cases}, \; r = 1,2,\cdots,N, \quad (3)$$

where S_z and H_{st} are the depth and altitude of the deep-towed seismic source at the current shot point, respectively; α and v_w are the seabed slope angle and seawater velocity at the current shot point, respectively; X_r and Z_r are the horizontal and vertical offsets of the rth receiver point from the shot point, respectively. $t_r^{D\_\mathrm{cal}}$, $t_r^{S\_\mathrm{cal}}$, and $t_r^{F\_\mathrm{cal}}$ are the theoretical traveltimes of the direct wave, sea-surface reflection, and seafloor reflection recorded at the rth receiver point, respectively; N is the total number of receiver points of the deep-towed seismic streamer; and X_r^*, Z_r^*, and H_{st}^* are intermediate quantities in the calculation.

For the slope angle α of the actual seabed topography, we first calculate the submarine depth at each shot point using depth and altitude measurements of the deep-towed seismic source. Subsequently, the submarine depth variation curve is fitted to a straight line within a specified calculation window. Typically, this window is set to a specific length, such as half the length of the deep-towed seismic streamer, along the horizontal survey line. The acquired straight line facilitates the calculation of the seabed slope angle related to each shot point through a sliding calculation window.

On the basis of Eqs. (2) and (3), the objective function for array geometry inversion in a deep-towed multichannel seismic exploration system under complex seabed topography conditions can be expressed as

$$\hat{\boldsymbol{\theta}} = \arg\min_{\boldsymbol{\theta}} \sum_{r=1}^{N} \left\{ (t_r^{D\_\mathrm{cal}}(\boldsymbol{\theta}) - t_r^{D\_\mathrm{obs}})^2 + (t_r^{S\_\mathrm{cal}}(\boldsymbol{\theta}) - t_r^{S\_\mathrm{obs}})^2 + (t_r^{F\_\mathrm{cal}}(\boldsymbol{\theta}) - t_r^{F\_\mathrm{obs}})^2 \right\}, \tag{4}$$

where $\boldsymbol{\theta} = [\theta_1, \theta_2, \theta_3, \cdots, \theta_N]^{\mathrm{T}}$ is the pitch angle of each line segment of the deep-towed seismic streamer; r is the receiver point number, and N is the total number of receiver points. $t_r^{D\_\mathrm{cal}}(\theta)$ and $t_r^{D\_\mathrm{obs}}$ are the theoretical and observed values of the direct wave traveltime recorded by the rth receiver point, respectively; $t_r^{S\_\mathrm{cal}}(\theta)$ and $t_r^{S\_\mathrm{obs}}$ are the theoretical and observed values of the sea-surface reflection traveltime recorded by the rth receiver point, respectively; and $t_r^{F\_\mathrm{cal}}(\theta)$ and $t_r^{F\_\mathrm{obs}}$ are the theoretical and observed values of the seafloor reflection travel time recorded by the rth receiver point.

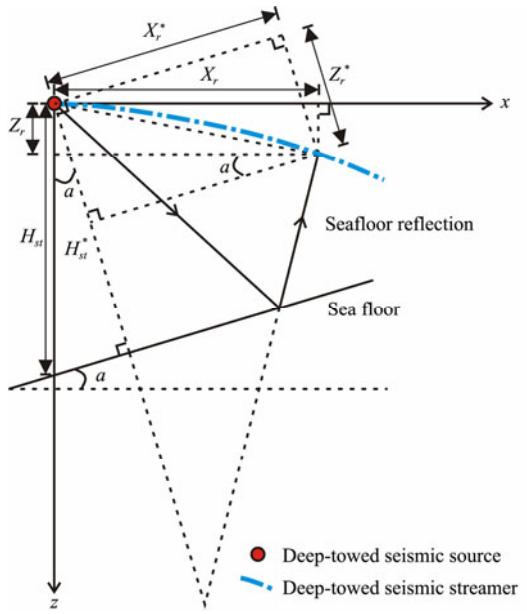

Fig.3 Schematic of the propagation path of the seafloor reflection of the deep-towed multichannel seismic exploration system.

Given the significant influence of seawater velocity on the accuracy of geometry inversion in a towed line array, particularly due to its lateral variation, we optimize v_w between 1480 m s^{-1} and 1500 m s^{-1}, as expressed in Eq. (5).

$$v_w = 1490 + 10\sin\theta_{N+1}. \tag{5}$$

On the basis of Eqs. (2)–(5), the particle swarm optimization algorithm is used to solve the objective function. The simultaneous inversion of the array geometry characterization parameters and the seawater velocity correction parameter can then be implemented to obtain accurate source-receiver positioning results for the deep-towed high-resolution multichannel seismic exploration system.

3 Numerical Experiments

To verify the effectiveness of the proposed method, we conduct numerical experiments by simulating the geometric shape of a towed line array during the operation of a deep-towed multichannel seismic exploration system. We generate 200 different array geometry models, each with randomly assigned model parameters, including seawater velocity, depth and altitude of the deep-towed source, and seabed slope angle.

Adhering to the engineering design parameters of the Kuiyang ST2000, the total number of receivers on the deep-towed seismic streamer is set to 48. The horizontal offset between the deep-towed source and the towing point of the seismic streamer is 2.0 m, with a vertical offset of 0.6 m. The interval distance between adjacent receivers along the cable is 3.125 m. To effectively characterize the geometric shape of the seismic streamer, the segment between the towing point and the first receiver point, spanning 12.5 m, is divided into four segments of 3.125 m each. Consequently, three pitch angles are added to the parameters for optimization ($\boldsymbol{\theta} = [\theta_1, \theta_2, \theta_3, \cdots, \theta_{52}]^{\mathrm{T}}$), where $\theta_1, \theta_2, \theta_3, \cdots, \theta_{51}$ are the pitch angles of the 51 segments of the deep-towed seismic streamer, and θ_{52} is the optimization parameter of the seawater velocity at the current shot point. The random geometry models of the towed line array (Fig.4) are generated by assigning pitch angles and introducing a random variable to the previous pitch angle. The range of this random variable is from −5° to 5°. Fig.5 displays the random values of the relevant working condition parameters for the 200 simulation models. Among these, the seawater velocity ranges from 1485 m s^{-1} to 1495 m s^{-1}, and the depth and altitude of the deep-towed seismic source range from 1000 m to 2000 m and from 100 m to 200 m, respectively. Considering the safety of the deep-towed multichannel seismic exploration system, the slope of the sea-

floor typically exhibits a gentle slope along the survey line, with the range of the submarine slope angle parameter spanning from −3° to 3°.

According to the parameters of the simulated geometry models of the towed line array, we calculate the travel times of direct waves, sea-surface reflections, and seafloor reflections. In practical scenarios, seismic travel time picking is susceptible to errors owing to the influence of the signal-to-noise ratio and source wavelet characteristics. To simulate this, picking uncertainties of 0.25, 0.50, 0.75, and 1.00 ms are intentionally introduced to the calculated seismic traveltimes in the experiment, with the travel time errors following a normal distribution. Fig.6 is the sketch map of the source and receiver positions for the No. 105 simulation model. The corresponding seabed slope angle is 2.31°, the source altitude is 137.09 m, and the seismic velocity of the seawater is 1488.54 $m\,s^{-1}$. Fig.7 shows the theoretical travel times and simulated travel time picking values under different picking uncertainties for the direct wave, seafloor reflection, and sea-surface reflection related to the No. 105 simulation model. Figs.7a−7d present the results under picking uncertainties of 0.25, 0.50, 0.75, and 1.00 ms.

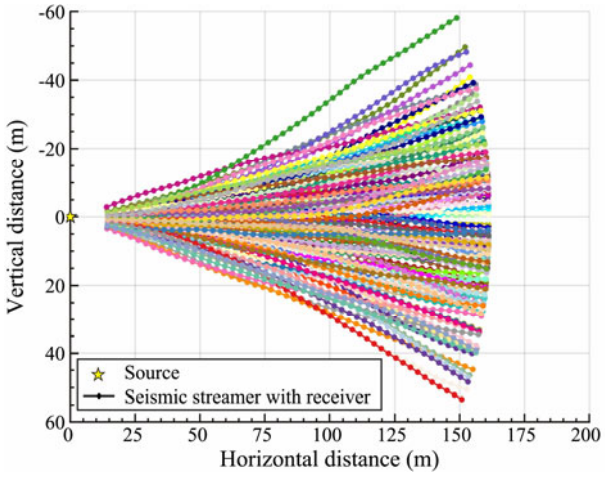

Fig.4 Schematic of the 200 randomly generated geometry simulation models of a towed line array. Different simulation models are color-coded.

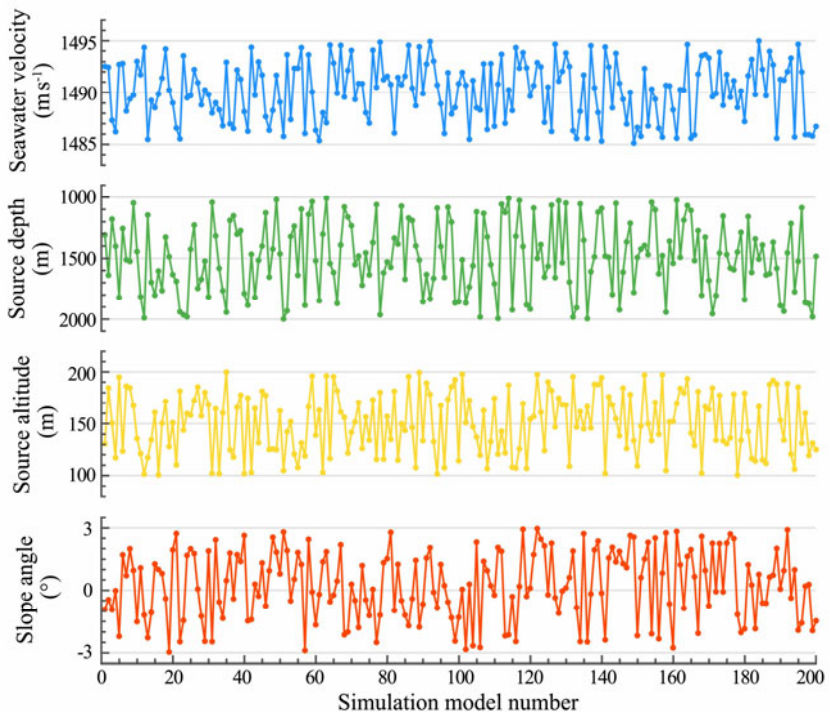

Fig.5 Random values for the relevant working condition parameters of the 200 simulation models. The blue, green, yellow, and red lines correspond to the seawater velocity, source depth, source altitude, and slope angle, respectively.

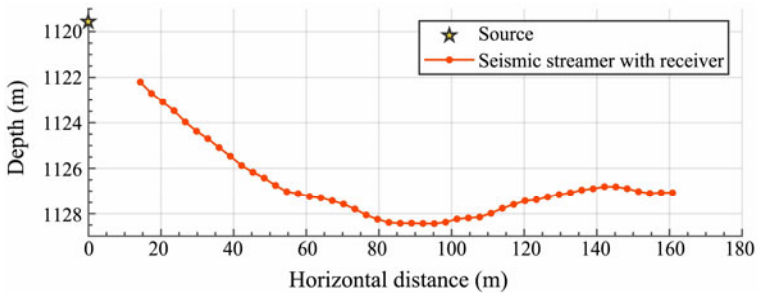

Fig.6 Plot of the source and receiver positions of the No. 105 simulation model. The red line represents the geometry of the deep-towed multichannel seismic streamer, and the dots are the 48 receivers along the streamer.

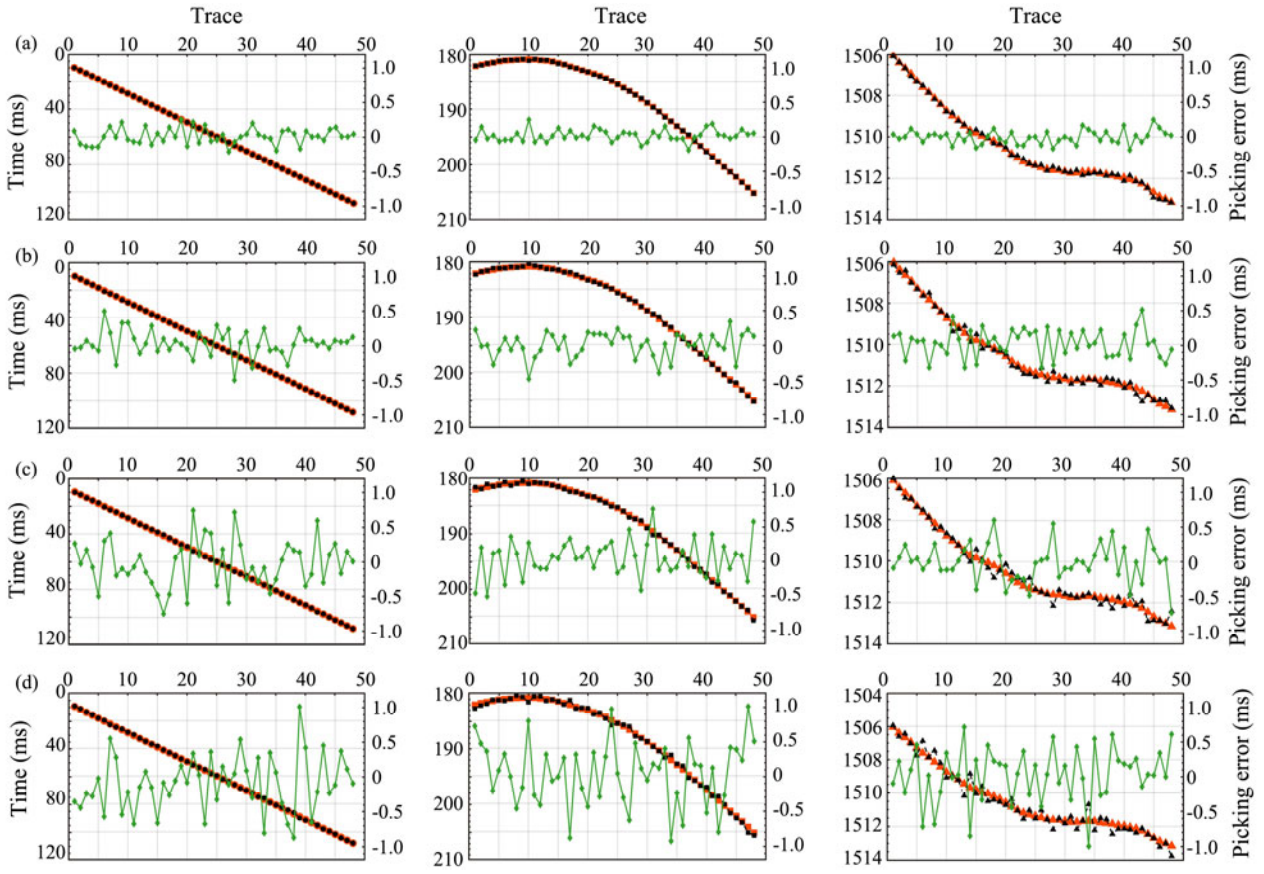

Fig.7 Simulated seismic traveltime picking under different picking uncertainties of (a) 0.25 ms; (b) 0.50 ms; (c) 0.75 ms, and (d) 1.00 ms. The red, black, and green lines are the theoretical travel times, travel time picking values, and relevant travel time picking errors, respectively. The dot, square and triangle represent the direct wave, seafloor reflection and sea-surface reflection, respectively.

Utilizing the simulated models and relevant traveltime picking data mentioned earlier, we employ five distinct inversion strategies to reconstruct the array geometry for all the simulation models. For ease of comparison in subsequent discussions, we assign names to the test groups corresponding to different inversion strategies. Group 1 employs a conventional method, utilizing accurate seawater velocity information. Group 2 adopts the same conventional method but assumes a fixed and inaccurate seawater velocity of 1490 m s^{-1}. In Group 3, the proposed method is utilized, with the removal of the seafloor reflection travel time error term from the objective function. The seawater velocity v_w is fixed at 1490 m s^{-1}, as in Group 2, mirroring Group 2 and disregarding variations in seawater velocity. Group 4 tailors the objective function of the proposed method for horizontal seabed conditions by setting the seabed slope angle α to 0°. Lastly, Group 5 implements the approach proposed in this study, which considers seawater heterogeneity and is suitable for a sloping seabed.

Fig.8 shows the results of geometric shape inversion for the No. 105 simulation model obtained using the aforementioned five inversion strategies. Figs.8a–8d depict the positioning outcomes of receivers under varying travel time picking uncertainties (0.25, 0.50, 0.75, and 1.00 ms). The corresponding analysis of positioning errors for each receiver point is presented in Fig.9. As shown in Figs.8 and 9, the seawater velocity of Groups 2 and 3 is 1490 m s^{-1}, but the actual velocity of this model is 1485.54 m s^{-1}. Therefore, inaccurate seawater velocity information leads to large positioning discrepancies between the calculated results and actual values. The average positioning error for receiver points in Groups 2 and 3 ranges from approximately 2.2 to 2.4 m. Conversely, Group 1, utilizing the real seawater velocity parameter, achieves positions close to reality. However, owing to the absence of considerations for fixed channel spacing and curvature smoothing in the deep-towed seismic streamer, Group 1 is susceptible to travel time picking errors. As the picking uncertainty increases, the fluctuation in the receiver point positioning errors becomes larger. Moreover, the conventional method employed in Group 1 fails to align with the actual scenario in the No. 105 simulation model, given the absence of accurate seawater velocity and seismic travel time picking values. The seabed of this model exhibits a known tilt with a slope angle of 2.31°. The inversion strategy of Group 4, tailored for horizontal seabed conditions, results in inaccurate seawater velocity and array geometry inversion outcomes. As the offset increases, positioning errors for far-offset receiver points become more pronounced, with an average positioning error of approximately 3.2 m for Group 4. Among the five test groups, the geometric shape inversion of Group 5 for the deep-towed seismic streamer aligns most closely with reality. The average positioning error for receivers in Group 5 is merely 0.29 m when the pick-

ing uncertainty is set to 1.00 ms. Consequently, the approach proposed in this study demonstrates commendable inversion accuracy, reliability, and an ability to address substantial travel time picking errors.

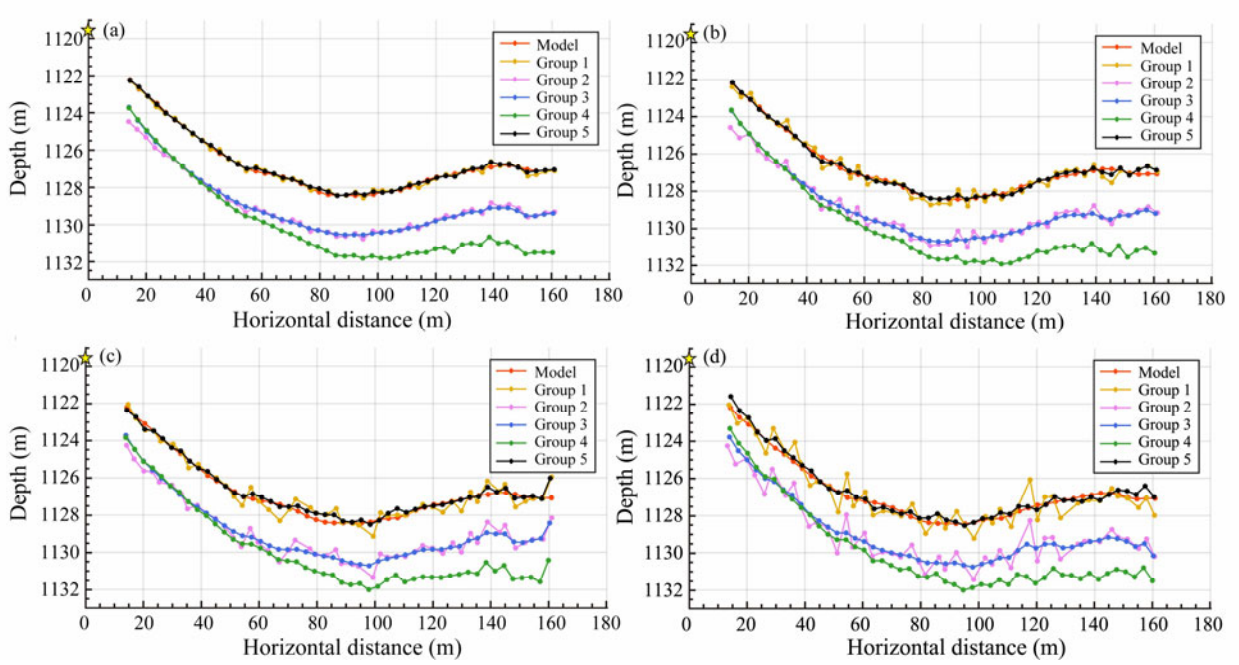

Fig.8 Comparison diagram of the array geometry inversion results of the No. 105 simulation model under different picking uncertainties of (a), 0.25 ms; (b), 0.50 ms; (c), 0.75 ms; (d), 1.00 ms.

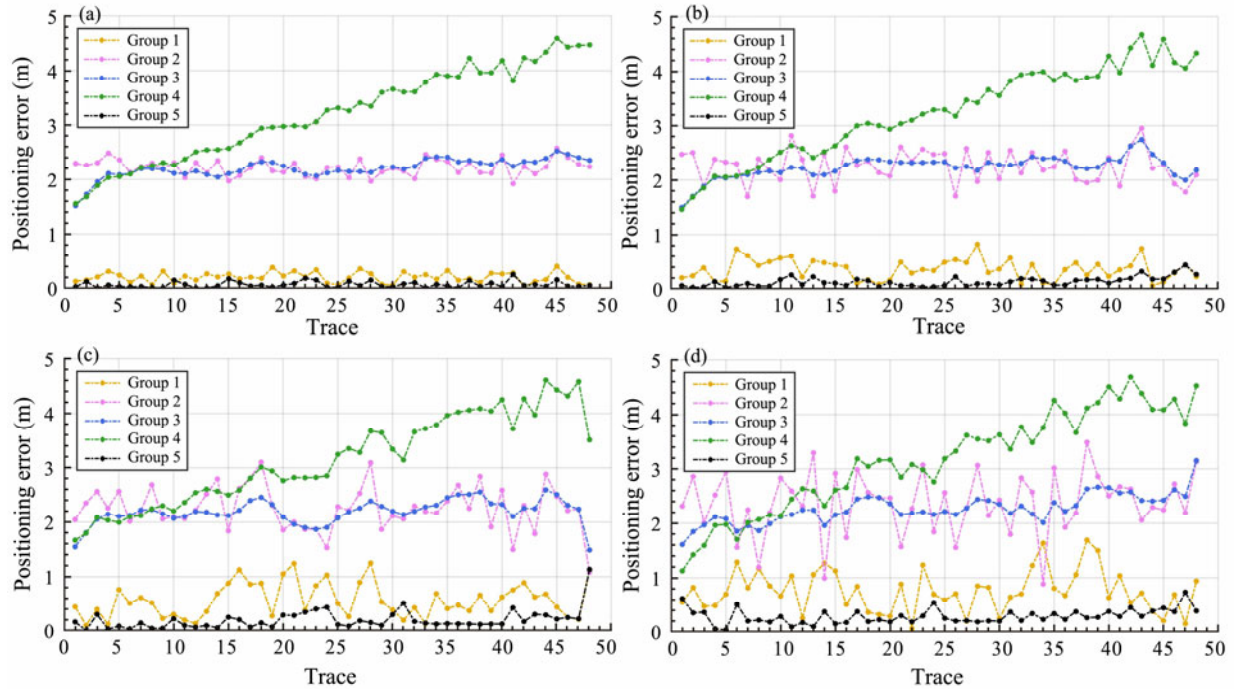

Fig.9 Comparison diagram of the receiver positioning errors of the No. 105 simulation model under different picking uncertainties of (a), 0.25 ms; (b), 0.50 ms; (c), 0.75 ms; (d), 1.00 ms.

Fig.10 compares the seawater velocity optimization results of the 200 simulation models under a picking uncertainty of 1.00 ms. When considering the randomly generated seabed slope angle cases depicted in Fig.5, we can see that although the seabed slope angle varies only between −3˚ and 3˚, the objective function applying only to the horizontal seabed assumption cannot guarantee the precision of the synchronous inversion of seawater velocity and source-receiver position.

The experimental results of the 200 simulation models are statistically analyzed, as shown in Fig.11. Fig.11a shows the average positioning error of the array geometry inver-

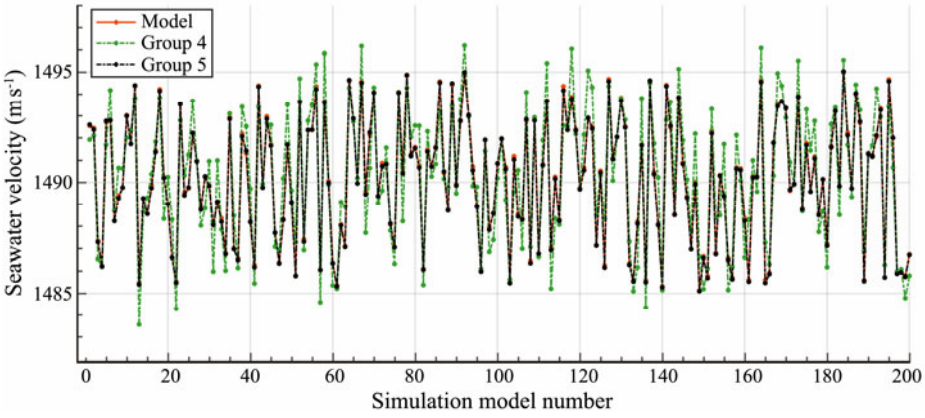

Fig.10 Seawater velocity optimization results under a picking uncertainty of 1.00 ms.

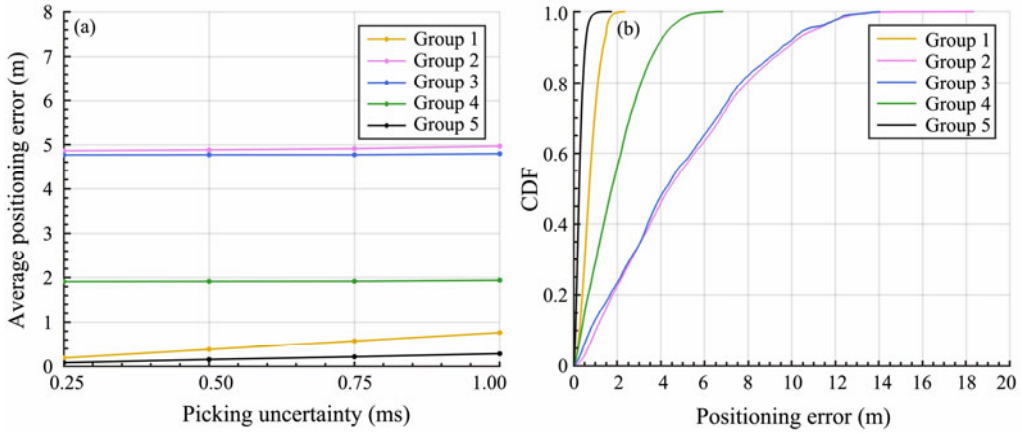

Fig.11 Statistical and comparative evaluation of simulation model test results. (a), the average positioning errors of receiver inversion results of all simulation models under different picking uncertainties; (b), the cumulative distribution function of positioning errors for different methods under a picking uncertainty of 1.00 ms.

sion results for all simulation models under different picking uncertainties. As an example, Fig.11b shows the cumulative distribution function of the positioning errors for receivers under different approaches, focusing on the results with a picking uncertainty of 1.00 ms. These findings in Fig.11 affirm that the proposed method, characterized by low dependence on both the initial model and travel time picking precision, proves applicable to the inversion of the geometric shape of the deep-towed seismic streamer under various working conditions. The inversion results exhibit high accuracy and stability.

4 Application Results

A large number of simulation model tests validate that the objective function formulated through the suggested method comprehensively considers the influences of the engineering design parameters of a deep-towed multichannel seismic exploration system, seawater heterogeneity, and seafloor topography. Thus, the particle swarm optimization algorithm is employed to solve the objective function, achieving source and receiver location information with high accuracy and reliability. The practical application data for this study are derived from a sea trial of the Kuiyang ST-2000 in the South China Sea. Part of the prestack shot gathers within the shot number range of 4780–5000 are utilized, with the relevant acquisition parameters detailed in Table 1. The deep-towed source energy is 3000 J, the shot interval is 6.25 m, the group interval is 3.125 m, the minimum offset is 14.5 m, the number of channels is 48, the record length is 3000 ms, and the sampling rate is 8 kHz.

Table 1 Sea trial acquisition parameters of the Kuiyang ST2000

Acquisition parameter	Value
Energy of source	3000 J
Shot interval	6.25 m
Group interval	3.125 m
Minimum offset	14.5 m
Number of channels	48
Record length	3000 ms
Sampling rate	8 kHz

Fig.12 shows the variation in depth and altitude of the deep-towed source corresponding to each shot point position. In the subsequent source-receiver positioning processing, the smoothed depth and altitude are adopted to calculate the seafloor depth variation, and the seabed slope angles corresponding to each shot point position are ac-

quired, as shown in Fig.13.

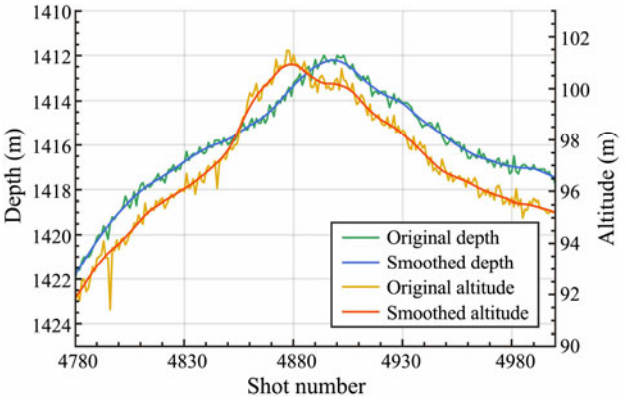

Fig.12 Variation curves of the deep-towed source depth and altitude.

Fig.14 shows the seismic travel time picking of partial shot gathers (shot numbers 4785, 4835, 4885, 4935, and 4985) from the experimental data. On the basis of the seismic travel time information, along with the depth and altitude of the deep-towed source and the seabed slope angle obtained from practical data, both conventional and proposed methods are employed to conduct source-receiver positioning of the deep-towed multichannel seismic exploration system. Fig.15 shows the final solution results of the geometric shape of the towed line array corresponding to the shot gathers in Fig.14, revealing distinctly different positioning results between the two methods. The geometric shape of the deep-towed seismic streamer, acquired using the proposed approach, exhibits a smoother curvature, aligning more closely with the actual circumstances. Furthermore, the average errors between the theoretical travel times calculated using the array geometry results via inversion of the proposed method and the practical travel time picking values of the direct wave, seafloor reflection, and sea-surface reflection are 0.22, 0.19, and 0.17 ms, respectively.

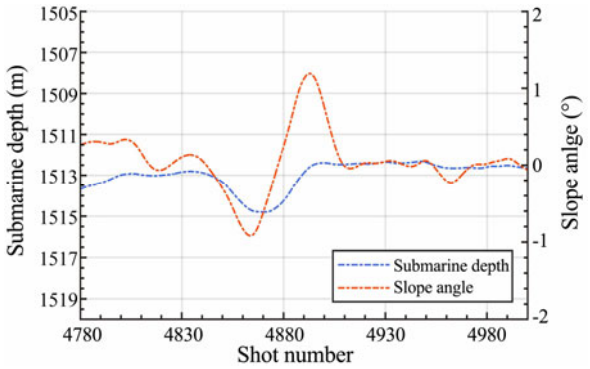

Fig.13 Variation in the seafloor depth and the estimation of the seabed slope angle.

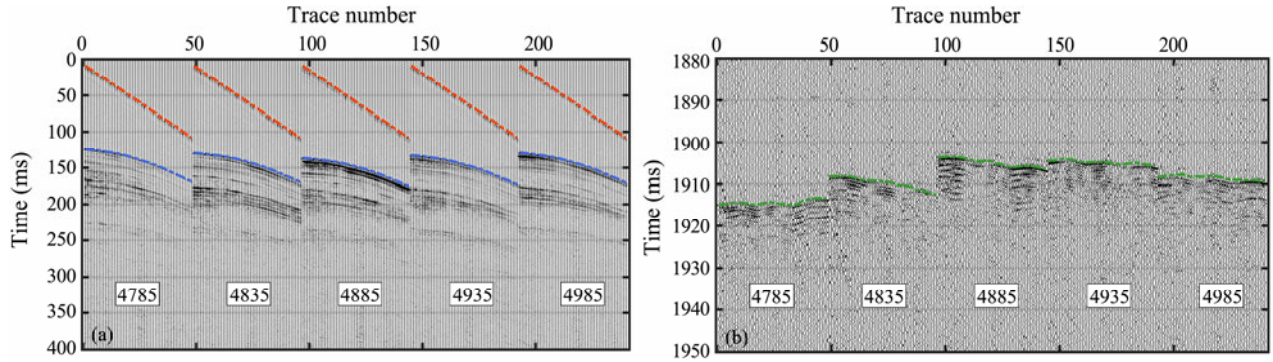

Fig.14 Partial prestack shot gathers of Kuiyang ST2000 and relevant travel time picking of the direct wave, seafloor reflection, and sea-surface reflection. The red, blue, and green dotted lines represent the travel time picking values of the direct wave, seafloor reflection, and sea-surface reflection, respectively.

In actual deep-towed seismic data processing, errors in travel time picking values are inevitable, especially for sea-surface reflections. As shown in Fig.14, the low signal-to-noise ratio of the sea-surface reflection poses challenges for accurate travel time picking. Consequently, the geometric shapes resulting from inversion using the conventional method exhibit non-smooth and distorted features (Fig.15). Additionally, owing to the constant seawater velocity assumed by the conventional method, the receiver positioning results show vertical offsets compared to the proposed method. The proposed approach, employing a nonlinear optimization algorithm, effectively addresses picking uncertainty, yielding a geometric representation of the deep-towed seismic streamer that aligns with objective reality. Considering the influence of seawater heterogeneity on inversion, the seawater velocity relevant to each shot gather is synchronously inverted, enhancing the precision of source-receiver positioning.

Utilizing the source-receiver positioning information obtained from both methods, floating datum correction (He *et al*., 2009) is applied to the deep-towed multichannel seismic prestack shot gathers, followed by velocity analysis. As shown in Fig.16, the velocity spectrum obtained using the proposed method exhibits superior focusing effects, contributing to the establishment of a refined velocity structure. Following normal moveout correction and stacking processing with the stacking velocity derived from the velocity spectrum, deep-towed seismic imaging profiles are generated (Fig.17). To facilitate a comparison of the two methods, no additional trim static correction or

poststack noise suppression is applied during processing, except for the time shift to the sea surface. The results affirm that the deep-towed seismic imaging profile obtained using the proposed method features clear and coherent events, evident wave group characteristics, and markedly improved signal-to-noise ratios and resolutions. However, acknowledging the residual moveout, attributed to factors like travel time picking errors, depth, and altitude measurement errors, neglect of receiver offsets from the source in the *y*-axis direction in 3D space, and others, these aspects must be addressed for further improvement. The primary contributor to residual moveout appears to be errors resulting from the approximate calculation of the seabed slope angle. Consequently, enhancing the applicability of the proposed method to significant changes in submarine topography and conducting follow-up research on geometric shape inversion for a deep-towed seismic streamer applicable to arbitrary seafloor morphology should be pursued in order to further enhance the accuracy and reliability of source and receiver positioning.

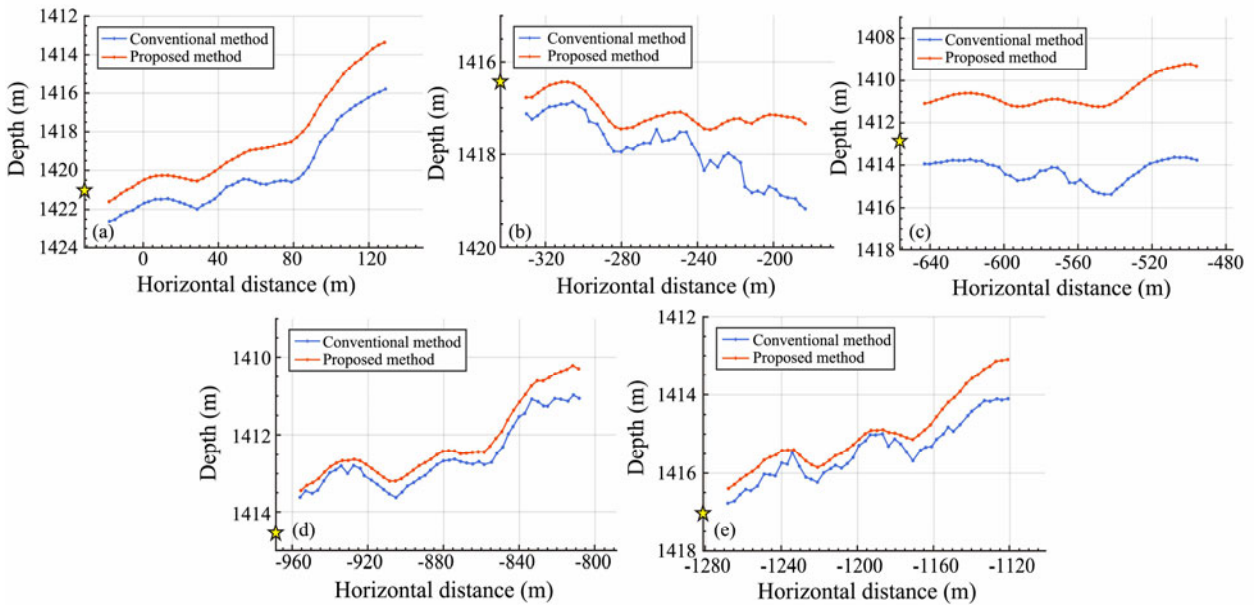

Fig.15 Geometric shapes of the practical data from inversion using the conventional and proposed methods. (a), shot number 4785; (b), shot number 4835; (c), shot number 4885; (d), shot number 4935; (e), shot number 4985.

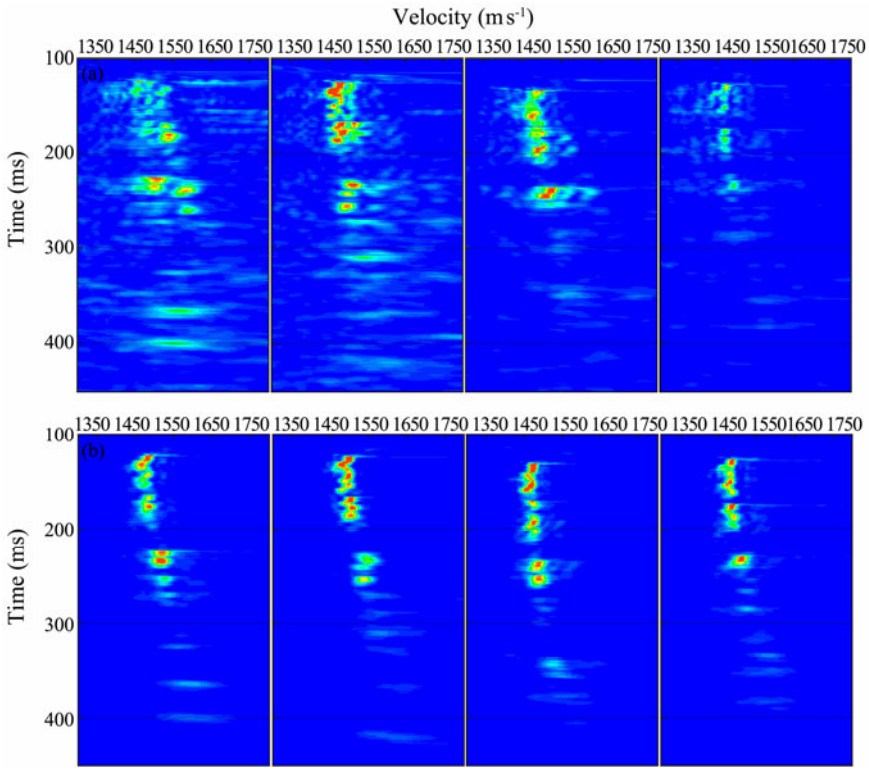

Fig.16 Velocity spectra of partial common midpoint gathers after floating datum correction using the source-receiver positioning results from (a) the conventional method and (b) the proposed method.

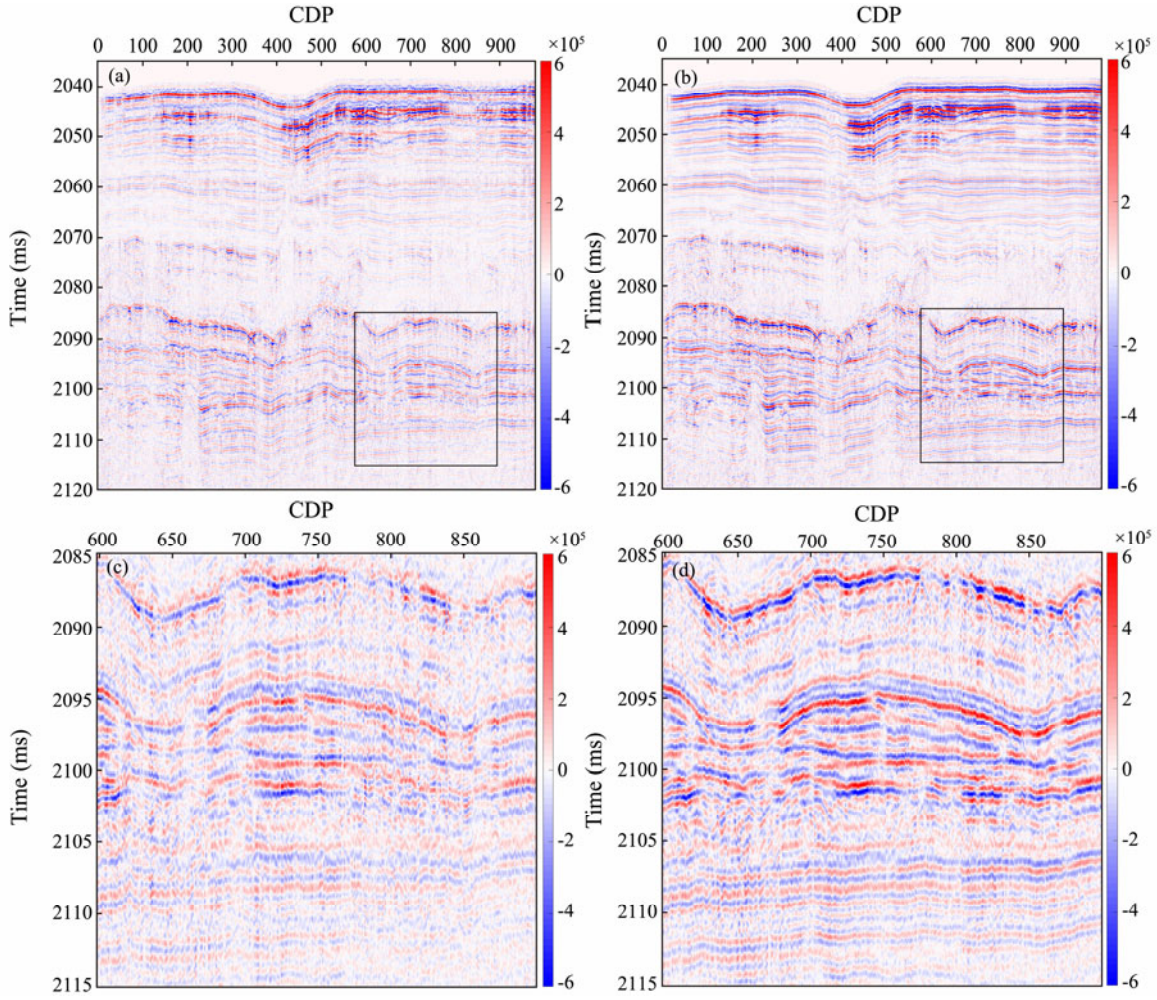

Fig.17 Deep-towed seismic imaging profiles of the experimental data comparing the quality of (a) the conventional method and (b) the proposed method. (c) and (d) are partially enlarged sections from (a) and (b), respectively.

5 Conclusions

In addressing the challenge of achieving precise source-receiver positioning for a deep-towed multichannel seismic exploration system, the comparative analysis of simulation models and practical data experiments between the conventional method and the approach proposed in this study leads to the following conclusions. The proposed method strategically decomposes the line array, consisting of a deep-towed seismic source and streamer, into multiple line segments. It characterizes the geometric shape of the towed line array based on the distances and pitch angles of these line segments. Consequently, the objective function constructed using this model aligns with objective reality and significantly enhances the accuracy and reliability of array geometry inversion, even in the presence of substantial picking uncertainty. Notably, the proposed method, free from the need for auxiliary information from attitude sensor measurements to address sensor drift and error accumulation, exhibits high inversion precision and stability. The consideration of lateral seawater velocity heterogeneity further contributes to its robust performance independently of the initial model. The study findings underscore the feasibility and applicability of the proposed procedure, particularly in addressing complex submarine topography conditions through the incorporation of seabed slope angle parameters.

Acknowledgements

The study is supported by the special funds of Laoshan Laboratory (No. LSKJ202203604), and the National Key Research and Development Program of China (No. 2016 YFC0303901).

References

Breitzke, M., and Bialas, J., 2003. A deep-towed multichannel seismic streamer for very high-resolution surveys in full ocean depth. *First Break*, **21** (12): 59-65.

Chapman, N., Gettrust, J., Walia, R., Hannay, D., Spence, G., Wood, W., *et al*., 2002. High-resolution, deep-towed, multichannel seismic survey of deep-sea gas hydrates off western Canada. *Geophycics*, **67** (4): 1038-1047.

Clare, M., Vardy, M., Cartigny, M., Talling, P., Himsworth, M., Dix, J., *et al*., 2017. Direct monitoring of active geohazards: Emerging geophysical tools for deep-water assessments. *Near Surface Geophysics*, **15**: 427-444.

Colin, F., Ker, S., and Marsset, B., 2020a. Fine-scale velocity distribution revealed by datuming of very-high-resolution deep-towed seismic data: Example of a shallow-gas system from

the western Black Sea. *Geophycics*, **85** (5): B181-B192.

Colin, F., Ker, S., Riboulot, V., and Sultan, N., 2020b. Irregular BSR: Evidence of an ongoing reequilibrium of a gas hydrate system. *Geophysical Research Letters*, **47** (20): 1-10.

Gettrust, J., Wood, W., and Spychalski, S., 2004. High-resolution MCS in deepwater. *The Leading Edge*, **23** (4): 374-377.

He, T., Spence, G., Riedel, M., Hyndman, R., and Chapman, N., 2007. Fluid flow and origin of a carbonate mound offshore Vancouver Island: Seismic and heat flow constraints. *Marine Geology*, **239**: 83-98.

He, T., Spence, G., Wood, W., Riedel, M., and Hyndman, R., 2009. Imaging a hydrate-related cold vent offshore Vancouver Island from deep-towed multichannel seismic data. *Geophysics*, **74** (2): B23-B36.

Hutapea, F., Tsuji, T., Katou, M., and Asakawa, E., 2020. Data processing and interpretation schemes for a deep-towed high-frequency seismic system for gas and hydrate exploration. *Journal of Natural Gas Science and Engineering*, **83**: 103573.

Ker, S., Le Gonidec, Y., and Gibert, D., 2012. Multiscale seismic attributes: Source-corrected wavelet response and application to high-resolution seismic data. *Geophysical Journal International*, **190** (2): 1746-1760.

Ker, S., Le Gonidec, Y., Marsset, B., Westbrook, G., Gibert, D., and Minshull, T., 2014. Fine-scale gas distribution in marine sediments assessed from deep-towed seismic data. *Geophysical Journal International*, **196**: 1466-1470.

Ker, S., Marsset, B., Garziglia, S., Le Gonidec, Y., Gibert, D., Voisset, M., *et al*., 2010. High-resolution seismic imaging in deep sea from a joint deep-towed/OBH reflection experiment: Application to a mass transport complex offshore Nigeria. *Geophysical Journal International*, **182**: 1524-1542.

Kong, F., He, T., and Spence, G., 2012. Application of deep-towed multichannel seismic system for gas hydrate on mid-slope of northern Cascadia margin. *Science China Earth Science*, **55** (5): 758-769.

Liu, H., Liu, H., Xing, L., and Li, Q., 2022. A new method for OBS relocation using direct water wave arrival time and accurate bathymetric data. *Marine Geophysical Research*, **43** (2): 1-17.

Marsset, B., Ker, S., Thomas, Y., and Colin, F., 2018. Deep-towed high resolution seismic imaging II: Determination of P-wave velocity distribution. *Deep-Sea Research I*, **132**: 29-36.

Marsset, B., Menut, E., Ker, S., Thomas, Y., Regnault, J. P., Leon, P., *et al*., 2014. Deep-towed high resolution multichannel seismic imaging. *Deep-Sea Research I*, **93**: 83-90.

Marsset, T., Marsset, B., Ker, S., Thomas, Y., and Le Gall, Y., 2010. High and very high resolution deep-towed seismic system: Performance and examples from deep water geohazard studies. *Deep-Sea Research I*, **57**: 628-637.

Pei, Y., Wen, M., Zhang, L., Yu, K., Kan, G., Zong, L., *et al*., 2022. Development of a high-resolution deep-towed multichannel seismic exploration system: Kuiyang ST2000. *Journal of Applied Geophysics*, **198**: 104575.

Riboulot, V., Cattaneo, A., Sultan, N., Garziglia, S., Ker, S., Imbert, P., *et al*., 2013. Sea-level change and free gas occurrence influencing a submarine landslide and pockmark formation and distribution in deepwater Nigeria. *Earth and Planetary Science Letters*, **375**: 78-91.

Riboulot, V., Ker, S., Sultan, N., Thomas, Y., Marsset, B., Scalabrin, C., *et al*., 2018. Freshwater lake to salt-water sea causing widespread hydrate dissociation in the Black Sea. *Nature Communications*, **9**: 117.

Rowe, M., and Gettrust, J., 1993. Fine structure of methane hydrate-bearing sediments on the Blake Outer Ridge as determined from deep-tow multichannel seismic data. *Journal of Geophysical Research*, **98** (B1): 463-473.

Talukder, A., Bialas, J., Klaeschen, D., Buerk, D., Brueckmann, W., Reston, T., *et al*., 2007. High-resolution, deep tow, multichannel seismic and sidescan sonar survey of the submarine mounds and associated BSR off Nicaragua Pacific margin. *Marine Geology*, **241**: 33-43.

Vanneste, M., Sultan, N., Garziglia, S., Forsberg, C., and L'Heureux, J., 2014. Seafloor instabilities and sediment deformation processes: The need for integrated, multi-disciplinary investigations. *Marine Geology*, **352**: 183-214.

Walia, R., and Hannay, D., 1999. Source and receiver geometry corrections for deep towed multichannel seismic data. *Geophysical Research Letters*, **26** (13): 1993-1996.

Wei, J., Liu, H., Xing, L., and Du, D., 2018. Application of seismic interferometric migration for shallow seismic high precision data processing: A case study in the Shenhu area. *Journal of Ocean University of China*, **17** (1): 46-52.

Wei, Z., Pei, Y., and Liu, B., 2020. A new deep-towed, multichannel high-resolution seismic system and its preliminary application in the South China Sea. *Oil Geophysical Prospecting*, **55** (5): 965-972 (in Chinese with English abstract).

Wood, W., Hart, P., Hutchinson, D., Dutta, N., Snyder, F., Coffin, R., *et al*., 2008. Gas and gas hydrate distribution around seafloor seeps in Mississippi Canyon, northern Gulf of Mexico, using multi-resolution seismic imagery. *Marine and Petroleum Geology*, **25**: 952-959.

Xing, L., Liu, X., Liu, H., Qin, Z., and Ma, B., 2021. Research on the construction of a petrophysical model of a heterogeneous reservoir in the hydrate test area in the Shenhu area of the South China Sea (SCS). *Geofluids*, **2021**: 5586118.

(Edited by Chen Wenwen)